

Minerva Access is the Institutional Repository of The University of Melbourne

Author/s:

Ye, L.;Xiao, P.;Scales, P.;Webley, P.;Singh, R.;Li, GK

Title:

Improved copper-based catalysts for alcohol-assisted CO₂ hydrogenation: A comparative study between novel nano-stabilized and deposition-precipitation method

Date:

2023-08-01

Citation:

Ye, L., Xiao, P., Scales, P., Webley, P., Singh, R. & Li, G. K. (2023). Improved copper-based catalysts for alcohol-assisted CO₂ hydrogenation: A comparative study between novel nano-stabilized and deposition-precipitation method. *Molecular Catalysis*, 547, pp.1-7. <https://doi.org/10.1016/j.mcat.2023.113289>.

Persistent Link:

<https://hdl.handle.net/11343/338646>

Improved copper-based catalysts for alcohol-assisted CO₂ hydrogenation: A comparative study between novel nano-stabilized and deposition-precipitation method

Linlin Ye,^a Penny Xiao,^a Peter Scales,^c Ranjeet Singh,^a Paul Webley,^b Gang Kevin Li^{*a}

^a Department of Chemical Engineering, The University of Melbourne, Parkville, VIC 3010, Australia

^b Department of Chemical and Biological Engineering, Monash University, Wellington Rd, Clayton VIC 3800, Australia

^c ARC Centre of Excellence for Enabling Eco-Efficient Beneficiation of Minerals, Department of Chemical Engineering, The University of Melbourne, Parkville, VIC 3010, Australia

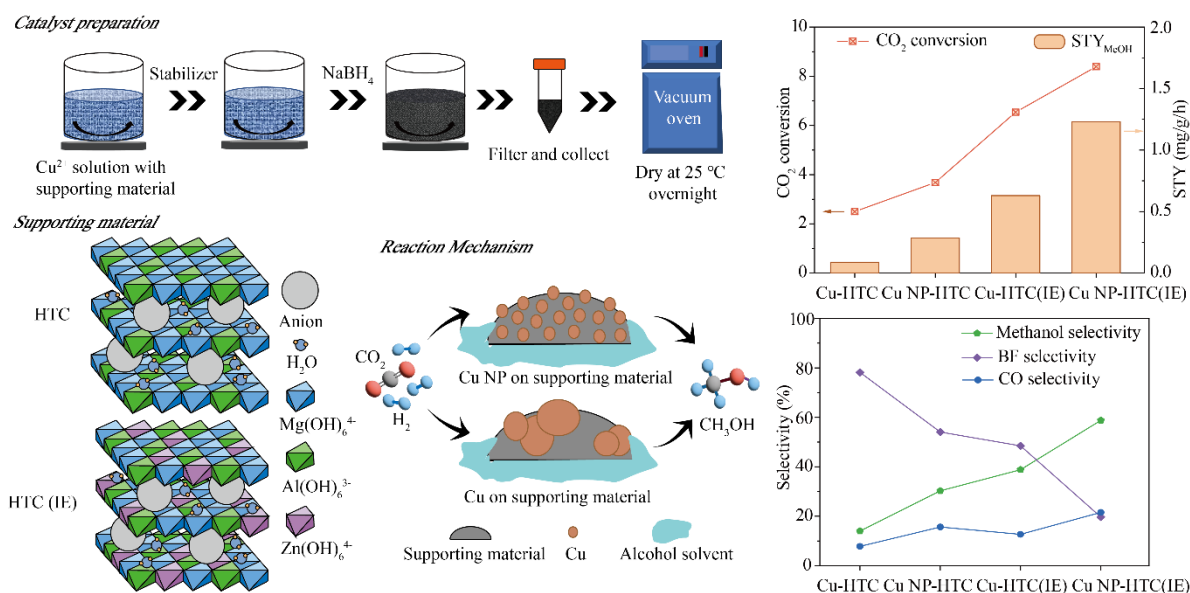
* Corresponding authors: li.g@unimelb.edu.au

Abstract

A growing awareness of the need to control the CO₂ concentration in the atmosphere spurs the demand for novel technologies to convert CO₂ to useful chemicals. Methanol as a high-quality liquid fuel is the main focus of CO₂ conversion and an active catalyst is the key for the methanol synthesis from CO₂ under mild reaction conditions. In this study, a new way of synthesizing catalysts with highly dispersed nano copper particles is reported and the characteristics of the nano catalysts compared with that of normal copper catalyst prepared using a deposition precipitation (DP) method. These copper-based catalysts can be well dispersed on layered hydrotalcite (HTC). The catalysts were prepared with the addition of a copolymer of polyethylene glycol and maleic acid (PEG-MA). This resulted in a significant decrease in particle size and exhibited efficient catalytic performance in a 1-butanol promoted CO₂ hydrogenation reaction at 170 °C, 3MPa. The work also confirms the status of Zn as an influential factor for methanol synthesis. The application of ion-exchange process and

stabilizers to catalyst preparation effectively improves the CO₂ conversion rate and the selectivity to methanol, which also inspires the development of catalysts from various fields.

Graphical abstract

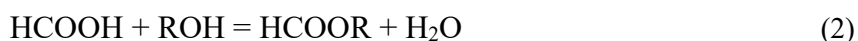


1. Introduction

According to the analysis from NOAA's global Monitoring Lab, the global average atmospheric CO₂ in 2022 was 421 ppm, setting a new historic record despite the continued economic drag from the COVID-19 pandemic[1]. CO₂ as a major component of greenhouse gases, is responsible for about two-thirds of the total heating influence generated from human activities[2]. Many researchers now are focusing on converting CO₂ to other value-added chemicals to form a win-win situation on economic and environmental factors.

Catalytic hydrogenation of CO₂ to methanol is widely considered to be a promising means of mitigating CO₂ emissions, since methanol is an important building block in a range of industries. Due to the chemically inert nature of CO₂, a thermodynamic barrier needs to be overcome by increasing the reaction temperature to at least 240 °C to facilitate CO₂ activation in the process of traditional CO₂ hydrogenation in a gas-phase reaction[3]. This results in a low CO₂ conversion and rapid deactivation of catalysts in the highly exothermic reactions. Fan et al[4] first proposed a new reaction route for methanol synthesis by the hydrogenation of carbon dioxide via formic ester based on the combination of a conventional Cu/ZnO catalyst and ethanol as a catalytic solvent at 443K and 30 bars pressure. The alcohol promotes methanol

synthesis by altering the reaction route (Eq.1-3), making methanol production at mild reaction conditions (423–443 K and 30-50 bars) practical. 1-butanol was chosen as the alcohol solvent for this project since it has a low vapour pressure under high temperatures and a high boiling point. It showed excellent performance in assisting the CO₂ hydrogenation to methanol reaction[5].



Metallic copper has been identified as the catalytically active component for methanol synthesis[6-8], and copper-based catalysts have already been widely used in industrial-scale methanol production[9, 10]. It is reported that the activity of copper-based catalysts is dependent on the dispersion of Cu nanoclusters on the support[11], while the size of Cu nanoclusters shows a strong correlation to its catalytic performance[12, 13]. Xiao et al[14] showed that the reduction of copper particle size from 28 nm to 6.5 nm increased CO₂ conversion from 2.5% to 10.7%. However, it is difficult to control the size of copper particles to the nano size due to aggregation tendency of all nanoparticles. One way to overcome this problem and synthesize a catalyst that is uniform in size, shape, composition is using additives that control particle dispersion and by implication, limit aggregation[15]. Water soluble polymers consisting of multiple repeating units can absorb quickly to the surface of metal preventing particle growth and overcoming any displacement stresses due to particle interactions. Many researchers have successfully synthesized Cu NPs by chemical reduction in Cu²⁺solutions in the presence of polymers [16]. Therefore, it shows promise as a method to synthesize effective copper-based methanol catalysts.

In this study, PEG-MA, a comb-graft copolymer was used as a stabilizer to control the size of copper particles supported on a commercial hydrotalcite (HTC, MG 50)[17, 18]. It is well known that a large specific surface area is beneficial for the dispersion of active metals, and the special structure of HTC for ion exchange make it a suitable support material for this research[19]. The cation ions in the Brucite-like layer of HTC can be exchanged with other divalent M²⁺ and trivalent M³⁺ ions. Natesakhawat et al[20]. found that the addition of ZnO to a copper-based catalyst can create a special site that acts as a CO₂ adsorption site at the interface of the Cu/ZnO, further improving the catalytic performance of Cu NP catalyst. Zn²⁺ was selected to proceed the ion exchange process with Mg²⁺ on a commercial HTC, synthesizing a new supporting material for Cu NP. The activity and structure of these novel Cu NP catalysts

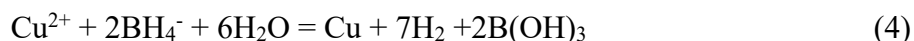
prepared through a new synthesizing route were explored and studied under mild reaction conditions (170 °C, 3Mpa) for the catalytic CO₂ hydrogenation reaction.

2. Experimental section

2.1 Catalyst preparation

2.1.1 Cu NP-HTC

The catalyst support material was a Mg/Al carbonate hydrotalcite namely PURAL MG50 (Al₂O₃: MgO 50: 50 wt.% ratio) purchased from SASOL. The HTC was first activated for 4 hours in air at 400 °C, and then it was added into a 3mmol/L CuSO₄·5H₂O solution and stirred for 1 hour to make a homogeneous slurry. PEG-MA comb polymer (addition rate of 20% of the copper mass) was then added to the mixture while vigorously stirring. The pH value of the mixture was adjusted using NaOH solution (0.1M) to ~7. After stirring for half an hour, excess NaBH₄ as a reducing agent, calculated based on 4 times molar ratio of copper (0.1M dissolved in methanol) was added dropwise into the mixture. The colour of the mixture changed from blue to brown, indicating the formation of Cu nanoparticles (Eq.4). Finally, the well-reduced mixture was filtered, washed with deionized water, and finally dried at room temperature under vacuum overnight. The whole synthesis process was carried out in an inert atmosphere(N₂) to prevent oxidation of the reduced nano Cu.



2.1.2 Cu-HTC

Cu-HTC catalysts were prepared by a deposition precipitation (DP) method[21] at room temperature. The activated HTC was added to 3 mmol/L CuSO₄·5H₂O solution and stirred for half an hour to make a homogeneous slurry at room temperature. K₂CO₃ solution (1.2 mol/L) was added dropwise to the suspension under vigorous agitation to adjust the pH value to approximately 10 and the mixture was stirred for another 2 hours. After that, the precursors were gathered by centrifugation, washed with deionized water until the pH was 7, and dried at 120 °C overnight. The dried sample was calcined at 350 °C in air to obtain CuO-HTC. Finally, the reduction process for CuO-HTC was conducted in a tube furnace in 5% H₂/Ar (Coregas) flow for 6 hours at 350 °C.

2.1.3 Supporting material HTC(IE)

A proportion of Mg^{2+} or Al^{3+} in the Brucite-like layer of HTC is exchangeable with a variety of divalent M^{2+} and trivalent M^{3+} ions with similar ionic radii to those of Mg^{2+} and Al^{3+} , respectively. The activated HTC was added to 0.1 mol/L zinc nitrate solution and stirred at 80 °C for 6 hours. The liquid mass to solid mass ratio was 40. After stirring, the suspension was collected and dried in flowing air at 110 °C for 20 hours and then ground into a fine powder. The supporting material was labelled as HTC (IE).

2.1.4 Cu NP- HTC(IE)

The synthesis process for Cu nano supported on HTC (IE) was the same as that of Cu NP-HTC, only the supporting material was changed from HTC to the pre-prepared HTC(IE).

2.1.5 Cu-HTC(IE)

The synthesis process for Cu nano supported on ion-exchanged HTC was same as that of Cu - HTC only the supporting material was changed from HTC to the pre-prepared HTC(IE).

2.2 Characterization of catalysts

The thermal stability of the catalysts and supporting material HTC were measured on a thermal gravimetric analyzer (TGA; TGA/SDTA851e, Mettler). The tested temperature was from 50-750 °C with a ramp rate of 5 °C/ min.

H_2 -TPR measurements were performed on a BELCAT-M (MicrotracBEL) to measure the reducibility of the catalysts. 20 mg of sample was first placed in a U-tube quartz reactor and swept with He to eliminate possible impurities at 200 °C for 2 h. After cooling, the samples were heated to 350 °C at a rate of 10 °C/min in H_2 /Ar (Coregas) mixture. The signal was recorded by mass spectrometry (BELMass, MicrotracBEL).

The basicity of the prepared catalysts was measured using a CO_2 temperature programmed desorption (CO_2 -TPD) method (BELCAT-M, MicrotracBEL). First, pure Ar (Coregas) was introduced to remove the moisture and other adsorbed molecules at 300 °C for 2 hours and then cooled to 40 °C. Subsequently, CO_2 was introduced to the reactor at 120 °C for 1 hour at a flow rate of 30 ml/min. The desorption process was performed by heating the sample at a rate of 5 °C/min from 25 °C to 350 °C in Ar. The desorbed CO_2 was also detected by mass spectrometry (BELMass, MicrotracBEL).

The dispersion of Cu (D_{Cu}) and the exposed Cu surface area (S_{Cu}) were determined by dissociative N_2O adsorption and performed on a BELCAT-M, MicrotracBEL. The sample was

first reduced in 5% H₂/Ar flow (30 mL/min) for 4 h at 300 °C, and the amount of hydrogen consumption was denoted as X. After reduction, the sample was cooled to 25 °C in Ar and maintained for 30 min. Subsequently, the sample was exposed to 5 % N₂O/He at 50 °C for 1 h to ensure that the metallic copper Cu⁰ was completely oxidized to Cu⁺. The oxidized sample was purged in Ar to remove residual N₂O and cooled to room temperature. Finally, 5% H₂/Ar was introduced to the reactor to reduce the Cu₂O to metallic Cu with a temperature programed to increase to 500 °C at a ramp rate of 5 °C/min. The amount of H₂ consumption in this part was denoted as Y.

$$D_{\text{Cu}}(\%) = \frac{2Y}{X} \times 100\% \quad (5)$$

$$S_{\text{Cu}}(\text{m}^2/\text{g}) = \frac{2Y \times N_a}{N \times m} \times 100\% \quad (6)$$

where D_{Cu} is the dispersion of Cu, S_{Cu} is the exposed copper surface area per gram catalyst, N_a is the Avogadro's constant (6.022 × 10²³ mol⁻¹), N (1.47 × 10¹⁹) is the number of metallic Cu atoms per square meter and m is the amount of catalyst. The experimental error in S_{Cu} and D_{Cu} was estimated at ±1% from three repeat steady-state measurements[22, 23].

The phase analysis and crystal size were investigated by X-ray diffraction with Cu-Kα radiation (XRD, Bruker AXS, D8 Advance). The XRD pattern was collected in 2θ ranging between 20 ° and 80 °. Cu crystallite size was calculated by the well-known Scherrer formula as given:

$$d_{\text{Cu}} = \frac{k\lambda}{\beta \cos \theta} \quad (7)$$

where D is particle size in nm, λ refers to X-ray wavelength (1.5418 nm), θ is Bragg angel and β represents half maximum width of the selected peak.

Scanning electron microscopy (SEM) (FEI Quanta 650F ESEM) equipped with an energy-dispersive X-ray spectroscopy source (EDX) was used to determine the morphology, size distribution, and composition of the nanoparticles.

The BET surface area, pore volume and pore size of the catalysts were determined by N₂ adsorption and desorption isotherms at 77K using a constant-volume adsorption apparatus (Micromeritics, ASAP 2020). The Barret-Joyner-Halenda (BJH) method applied to the N₂ adsorption data evaluated porosity distribution.

2.3 Evaluation of catalytic performance

Activity studies of the catalysts were performed in a batch reactor as shown in Figure S1 for CO₂ hydrogenation to methanol. A leakage test was performed each time prior to experiments for safety reasons. The catalyst was ground and sieved to 100 μm for each experiment. 1.5g of the synthesized catalyst was loaded into the reactor cell containing 50mL 1-butanol in an argon glove box to avoid catalyst oxidation. The whole reaction apparatus was evacuated to remove air first and then the reactor was pressurized with the feed gas (CO₂: H₂=1:3). Each batch proceeded at 170 °C, 3 MPa, under vigorous stirring at 600 rpm for 24 h. The pressure and temperature data during the reaction process was recorded automatically via LabVIEW software. Both liquid and gas samples were analyzed on a gas chromatograph (GC7890B, Agilent) equipped with a thermal conductivity detector (TCD) and flame ionization detector (FID). The catalytic performance was reported in terms of CO₂ conversion (X_{CO_2}), space-time yield of methanol STY_{MeOH} , methanol selectivity (S_{MeOH}), and CO selectivity (S_{CO}).

$$X_{CO_2} = \frac{\text{mol of C in final products} \times 100\%}{\text{mol of CO}_2 \text{ feed}} \quad (8)$$

$$STY_{MeOH} = \frac{\text{mol of methanol product} \times M_{MeOH}}{\text{mass of catalyst (g)} \times \text{reaction time (h)}} \quad (9)$$

$$S_{MeOH} = \frac{\text{mol of methanol product} \times 100\%}{\text{mol of all products}} \quad (10)$$

$$S_{CO} = \frac{\text{mol of CO product} \times 100\%}{\text{mol of all products}} \quad (11)$$

3. Results and discussion

3.1 Structural and morphological characterization

Scanning electron microscopy (SEM) and energy-dispersive X-ray spectroscopy (EDX) were conducted to explore the structure of HTC after the ion-exchange process as described in 2.1.3. The SEM images shown in Figure 1 demonstrate that the morphology of HTC before and after the ion exchange process remains stable, which indicates the exchange of Mg²⁺ cations in the HTC layer with Zn²⁺ does not affect the structure of HTC. Elemental analysis conducted by EDX is shown in Table S1. Before the ion-exchange process, no Zn could be detected, while

after the process, the Zn weight percentage was 34.53% and the Mg/Al atom ratio changed from 1.34 to 0.91, indicating partial replacement of Mg by Zn.

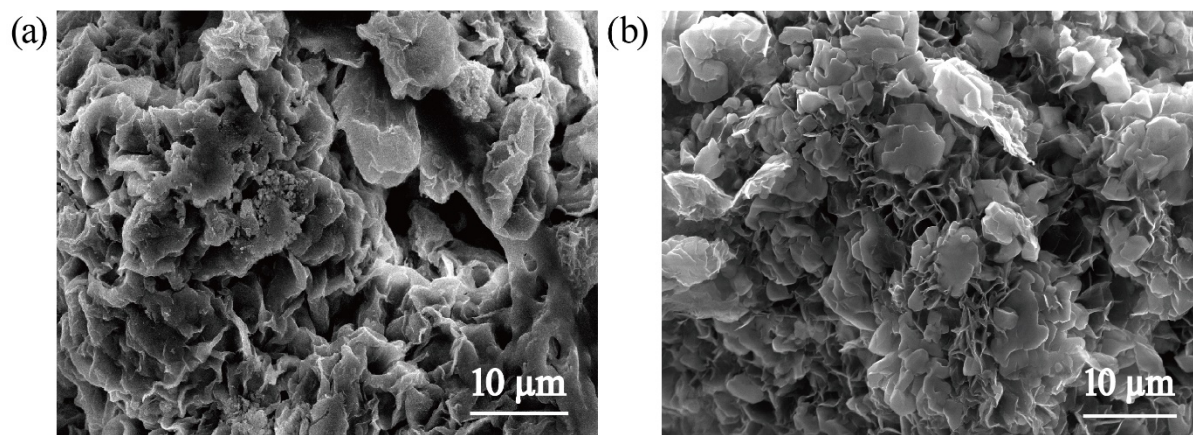


Figure 1. SEM images of HTC structure. a) before ion exchange. b) after ion exchange.

The thermal stability of catalysts and supporting materials was studied by thermogravimetric analysis (TGA) and derivative thermogravimetry (DTA), and the profiles are shown in Figure 2. The weight loss was 16% for the original supporting material HTC in the tested temperature zone, and three main weight loss stages were observed in all the tested samples. The first stage appeared below 200 °C and accounted for 2-5% of weight loss due to the elimination of physically adsorbed and interlayer water. The weight loss in the second stage was between 200 to 400 °C ascribed to the removal of hydroxyl groups and carbonate anions in the brucite-like layers. When the temperature was above 400 °C, the third stage of mass loss occurred due to the decomposition of carbonate anions in the interlayer region[24]. The stability of the supporting material HTC after ion-exchange was improved (Figure 2d), and the Cu NP-HTC(IE) catalyst showed the highest stability of all the tested samples (Figure 2f). Since the reaction temperature utilized herein was 170 °C, the mass loss for all the catalysts was less than 5%.

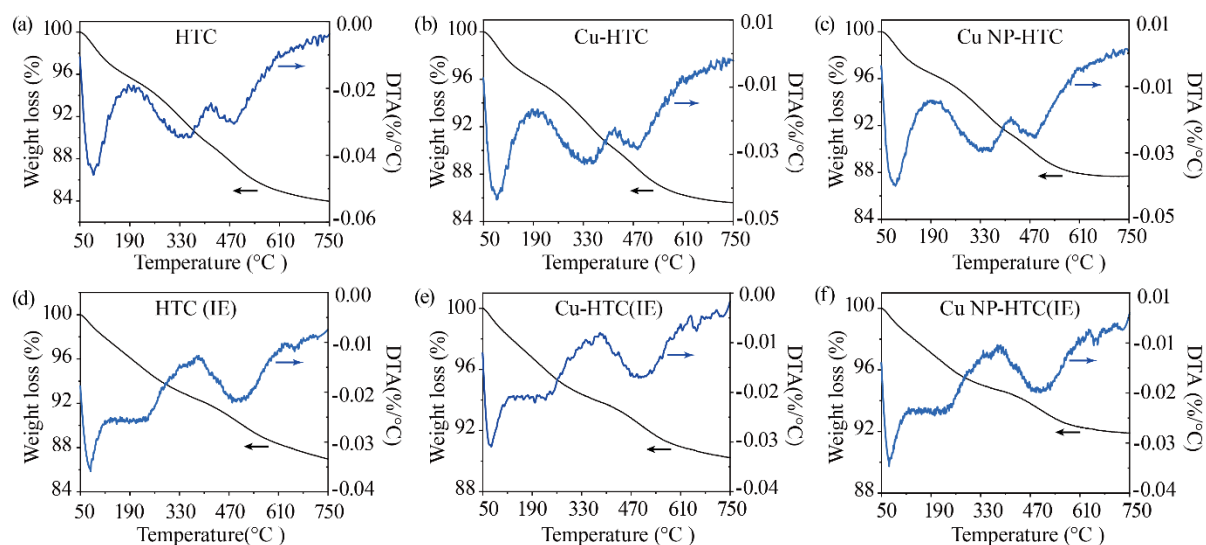


Figure 2. TGA-DTA profiles of a) HTC, b) Cu-HTC, c) Cu NP-HTC, d) HTC(IE), e) Cu-HTC(IE), f) Cu NP-HTC(IE).

The reduction behaviour of the catalysts made by the deposition precipitation method was evaluated using H_2 -TPR experiments. From the profiles shown in Figure S2, the reduction peaks were both in the range from 150 to 300 °C, so the reduction temperature was chosen as 350 °C for the catalysts to ensure completely reduction of Cu^{2+} to metallic Cu^0 . The reduction peak of Cu-HTC(IE) shifted to a lower temperature indicating that the incorporation of Zn favors the reduction behavior of Cu^{2+} [25].

Basic sites on the catalysts play a crucial role in CO_2 adsorption and activation, which is one of the most important processes in CO_2 hydrogenation to methanol. The reaction temperature in this project was below 200 °C and the strong basic sites appeared above 450 °C, attributed to the existence of low-coordination oxygen anions. The basic sites below 450 °C are therefore classified as weak and moderate basic sites, symbolized as α and β respectively. The weak basic sites (α , peak at 200 °C) were attributed to CO_2 binding over the surface OH^- group and moderate basic sites (β , peak at 270 °C) were ascribed to CO_2 binding over unsaturated metal–oxygen pairs[26]. Figure 3 indicates that the introduction of Zn to the supporting material significantly increases the intensity of basic sites, which contributes to easier CO_2 adsorption and activation[27].

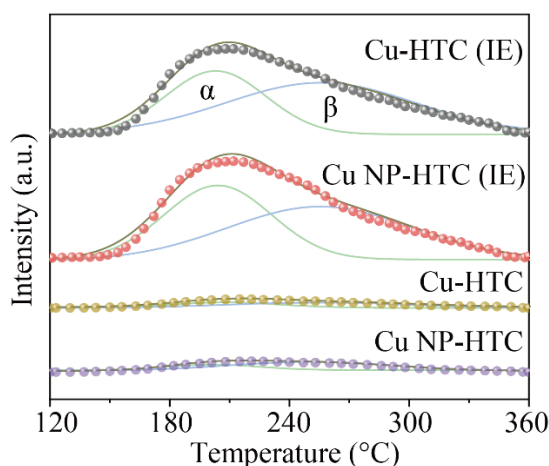


Figure 3. CO₂-TPD profiles of the catalysts

The XRD patterns for the various reduced catalysts are shown in Figure 4. Diffraction peaks assigned to Cu (JCPDS card No. 85-1326) are observed at about 43.5° (111), 50.4° (200) and 74.2° (220) in all the copper-based catalysts indicating that copper was successfully loaded onto the supporting material and reduced to Cu⁰. The peak pattern of the HTC(IE) sample showed obvious peaks for ZnO (JCPDS card No. 80-0074) compared with the original HTC sample, demonstrating a successful ion-exchange process. The Cu-HTC(IE) and Cu NP-HTC(IE) catalysts both showed the existence of Cu and ZnO, while the peak pattern of Cu NP-HTC(IE) was not as obvious as that of Cu-HTC(IE). It is hypothesised that this is due to the higher level of dispersion of the copper particles prepared by the new synthesis route. The magnitude of the crystallite size of Cu (d_{Cu}) was calculated based on the full width at half maximum of the strongest diffraction peak at 43.5° (111) using the Scherrer equation and is shown in Table 1.

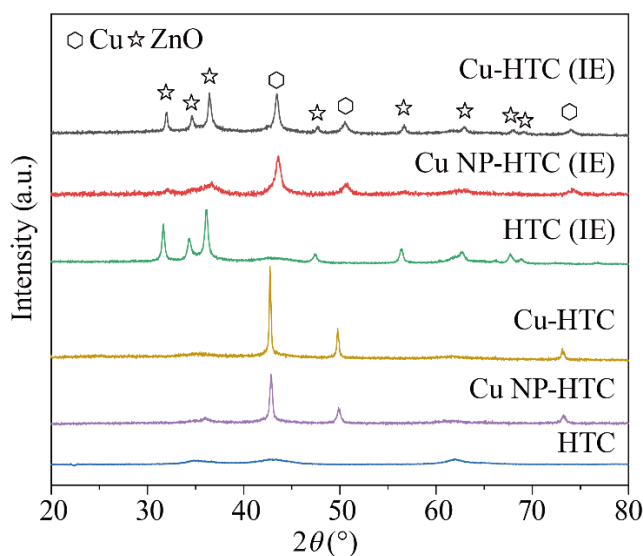


Figure 4. XRD patterns for various reduced Cu based catalysts

The specific surface area and pore structures for these catalysts obtained from N₂-physisorption are presented in Table 1. It is observed that the surface area of nano Cu catalysts was higher than that of Cu catalyst loaded on the same supporting material prepared by the traditional precipitation method, while the crystallite size of copper measured by XRD was smaller in nano catalysts, showing an opposite trend compared with the BET surface area. The increased surface area and decreased copper particle size in nano catalysts exhibited is attributed to the PEG-MA polymer preventing particle size growth, providing more active sites for CO₂ conversion. From the data presented in Table1, it is shown that the catalysts with smaller copper particle size exhibited a higher S_{Cu} and D_{Cu}, which implies copper particle size is a strong influencing factor in S_{Cu} and D_{Cu}[26].

Table 1. Physicochemical properties of reduced catalysts.

Subject	BET surface area (m ² /g)	Pore volume (cm ³ /g)	Pore size (nm)	Average particle size (nm)	d _{Cu} ^a (nm)	D _{Cu} ^b (%)	S _{Cu} ^b (m ² /g)
Cu-HTC	75.99	0.14	9.89	78.95	33.74	3.44	22.34
Cu NP-HTC	102.3	0.14	9.72	58.66	22.08	6.19	40.19
Cu-HTC (IE)	116.3	0.24	10.84	56.31	14.71	8.20	53.24
Cu NP-HTC (IE)	171.0	0.28	9.95	35.09	10.01	18.61	89.41

^a Calculated by the Scherrer equation based on the diffraction peak of Cu at $2\theta = 43.5^\circ$ (111)

^b D_{Cu}, S_{Cu} calculated from N₂O chemisorption

The morphologies of catalysts prepared through different processes is shown in SEM images in Figure 5. Copper particles of the catalysts synthesized with the addition of polymer were more uniformly distributed on the supporting material and maintained at a smaller size, much less than 100nm, presenting a perfect nano-morphology (Figure 5b and 5d). In contrast, the catalysts prepared by the DP method, the copper particles were aggregated to form large bulk particles (Figure 5a and 5c). The difference between the supporting material HTC and HTC (IE) was not an influencing factor of catalyst morphology in this project. The metal components on the surface of catalysts obtained from EDX analysis are presented in Figure 5e. The copper weight percentages detected by EDX in all catalysts were consistent with the initial calculated addition about 20 wt.%, and since Mg and Al have already been shown to not be the main

influencing factors in the catalytic methanol synthesis reaction, the weight percentages of copper and zinc were the main indicators. The zinc component on the surface of catalysts supported by HTC(IE) could be easily detected by EDX, further confirming the success of zinc addition through ion exchange process.

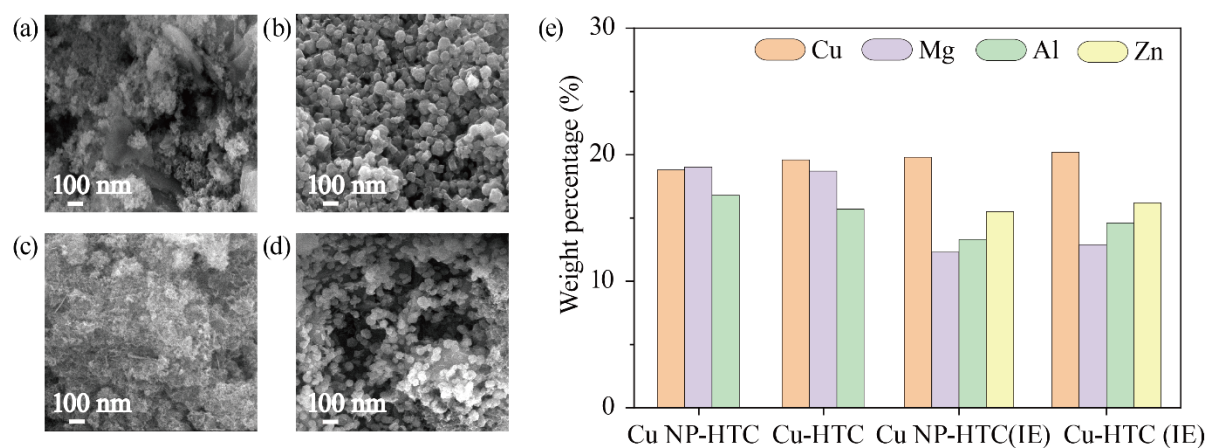


Figure 5. SEM images and EDX analysis of catalysts: a) Cu-HTC; b) Cu NP-HTC; c) Cu-HTC(IE); d) Cu NP-HTC(IE); e) weight percentages of metal components detected on the surface.

3.2 Catalytic activity of Cu nano catalysts

The catalytic activity of these copper-based catalysts was evaluated for CO₂ conversion to methanol with the assistance of 1-butanol solvent in the batch reactor (Figure S1). Based on the results obtained from GC and the reaction equation (1) to (3), the only intermediate liquid phase product that could be detected was butyl formate (BF). The reverse water-gas shift reaction (RWGS) was a common second reaction that occurred during the catalytic CO₂ hydrogenation to methanol reaction, which produced CO as a gaseous by-product. The CO₂ conversion rates and space time yield (STY) of methanol at 170 °C, 3MPa in the batch reactor with different catalysts are shown in Figure 6a. For the catalysts with same supporting material and copper weight percentage, the catalyst with copper nanoparticles (Cu NP-HTC and Cu NP-HTC(IE)) clearly showed better performance in terms of CO₂ conversion and STY_{Methanol} compared with Cu-HTC and Cu-HTC(IE) respectively. This reflects the advantages of the new Cu nano catalyst preparation methodology inclusive of the addition of PEG-MA. It also verifies the effect of copper particle size on CO₂ conversion. Generally, the conversion of CO₂ needs efficient adsorption and activation of both H₂ and CO₂ on the catalyst surface[28], so the low CO₂ conversion over metallic Cu was mainly ascribed to weak CO₂ adsorption ability[29] without a ZnO promoter. With the addition of ZnO, both the CO₂ conversion and

STY_{MeOH} of the same catalyst were improved, and the catalyst Cu NP-HTC (IE) showed the highest CO₂ conversion rate and STY_{MeOH} among all the tested catalysts.

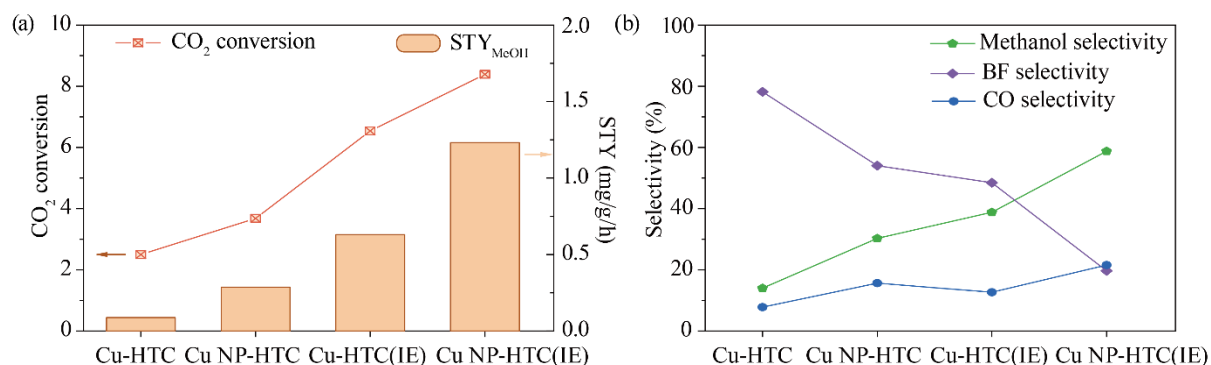


Figure 6. Catalytic performance of catalysts. a) CO₂ conversion and space time yield (STY) of methanol. b) Selectivity of final products

As for the selectivity for all the products final obtained after the alcohol assisted CO₂ conversion reaction, it is observed that for the catalysts without Zn as a promoter, the selectivity for methanol was quite low. ZnO provides active sites for hydrogen spill-over, and serves as a reservoir for atomic hydrogen[30], facilitating the reactions described in Eq.1 and Eq.3, leading to enhanced CO₂ conversion and methanol selectivity. With the help of nano Cu particle and Zn promoter, the selectivity for the only liquid intermediate product butyl formate (BF) decreased from nearly 80% to only 20%, contributing to the superior methanol selectivity (64%) of the Cu NP-HTC (IE) catalyst. Interestingly, the CO selectivity was higher with copper nano catalysts which indicated the small Cu particle size and good dispersion also facilitated CO formation[31].

4. Conclusions

Several types of copper-based catalysts with different particle sizes supported on a HTC material have been successfully synthesized for CO₂ hydrogenation to methanol and their catalytic efficiencies studied. In general, due to the indispensable roles of both Cu and Zn in the CO₂ hydrogenation reaction, the bimetallic material modified through an ion-exchange process for HTC showed a higher efficiency than the single metal materials supported on the original HTC in terms of CO₂ conversion and methanol selectivity. With the help of a dispersion controlling additive (PEG-MA), the precipitation of copper to the HTC surface achieved a small particle size, which further promoted the catalytic performance for both single metal Cu and bimetallic metal Cu/Zn oriented reactions.

Compared with the traditional catalyst preparation method, the new route of synthesizing copper-based catalyst proposed in this study saves energy consumption and reaction time and does not require high-temperature reduction of CuO to Cu. It provides a nano particle size and uniform distribution of the active metal component (copper) on the catalyst. The catalysts synthesized by the novel proposed preparation method combining copolymer stabilizer and an ion-exchange process on HTC support showed superior catalytic performance for CO₂ hydrogenation to methanol process compared with the catalysts prepared by a DP method with the same metallic composition. This catalyst preparation method can not only be applied to CO₂ hydrogenation reaction, but also can be used as a reference in other thermal catalytic reactions, benefiting all those focusing on catalyst synthesis and catalytic reactions.

Supporting Information

Supporting Information is available from the Wiley Online Library or from the authors.

Acknowledgments

The authors gratefully acknowledge the financial support of the China Scholarship Council (No.201706080002). This work was performed in part at the Materials Characterisation and Fabrication Platform (MCFP) at the University of Melbourne and the Victorian Node of the Australian National Fabrication Facility (ANFF). The authors would like to acknowledge the sponsor from Australia Research Council DP190101336. PJS acknowledges support of the Australian Research Council through the ARC Centre of Excellence for Enabling Eco-Efficient Beneficiation of Minerals, grant number CE200100009.

Conflict of Interest

The authors declare no conflict of interest.

References

1. González del Castillo, E., et al., *CO₂ variability in the Mexico City region from in situ measurements at an urban and a background site*. 2022. **35**(2): p. 377-393.
2. Aleixandre-Tudo, J.L., et al., *Trends in funding research and international collaboration on greenhouse gas emissions: a bibliometric approach*. Environmental Science and Pollution Research, 2021. **28**(25): p. 32330-32346.
3. Saeidi, S., et al., *Recent advances in CO₂ hydrogenation to value-added products - Current challenges and future directions*. Progress in Energy and Combustion Science, 2021. **85**.
4. Fan, L., Y. Sakaiya, and K. Fujimoto, *Low-temperature methanol synthesis from carbon dioxide and hydrogen via formic ester*. Applied Catalysis a-General, 1999. **180**(1-2): p. L11-L13.

5. H Nieminen, G.G., A Laari, T Koironen, *Alcohol promoted methanol synthesis enhanced by adsorption of water and dual catalysts*. 2018.
6. Cybulski, A., *Liquid-Phase Methanol Synthesis - Catalysts, Mechanism, Kinetics, Chemical-Equilibria, Vapor - Liquid Equilibria, and Modeling - a Review*. Catalysis Reviews-Science and Engineering, 1994. **36**(4): p. 557-615.
7. Joyner, R.W., et al., *The Influence of Precursor Structure and Composition on the Activity of Copper/Zinc Oxide Catalysts for Methanol Synthesis*. Catalysis Today, 1991. **10**(3): p. 417-419.
8. Liu, X.M., et al., *Recent advances in catalysts for methanol synthesis via hydrogenation of CO and CO₂*. Industrial & Engineering Chemistry Research, 2003. **42**(25): p. 6518-6530.
9. Kuld, S., et al., *Quantifying the promotion of Cu catalysts by ZnO for methanol synthesis*. Science, 2016. **352**(6288): p. 969-974.
10. Cui, X.T. and S.K. Kaer, *A comparative study on three reactor types for methanol synthesis from syngas and CO₂*. Chemical Engineering Journal, 2020. **393**.
11. Lam, E., et al., *Isolated Zr Surface Sites on Silica Promote Hydrogenation of CO₂ to CH₃OH in Supported Cu Catalysts*. Journal of the American Chemical Society, 2018. **140**(33): p. 10530-10535.
12. Zheng, L.P., et al., *Metal-organic framework derived Cu/ZnO catalysts for continuous hydrogenolysis of glycerol*. Applied Catalysis B-Environmental, 2017. **203**: p. 146-153.
13. Yuan, Z.L., et al., *Hydrogenolysis of glycerol over homogeneously dispersed copper on solid base catalysts*. Applied Catalysis B-Environmental, 2011. **101**(3-4): p. 431-440.
14. Xiao, S., et al., *Highly efficient Cu-based catalysts via hydrotalcite-like precursors for CO₂ hydrogenation to methanol*. Catalysis Today, 2017. **281**: p. 327-336.
15. Moshfegh, A.Z., *Nanoparticle catalysts*. Journal of Physics D-Applied Physics, 2009. **42**(23).
16. Feng, Z.V., et al., *Synthesis and Catalytic Evaluation of Dendrimer-Encapsulated Cu Nanoparticles An Undergraduate Experiment Exploring Catalytic Nanomaterials*. Journal of Chemical Education, 2009. **86**(3): p. 368-372.
17. Anderson, R., et al., *Concentrated synthesis of metal nanoparticles in water*. Rsc Advances, 2014. **4**(60): p. 31914-31925.
18. Anderson, R., et al., *Concentrated aqueous synthesis of nanoparticles using comb-graft copolymer stabilisers: the effect of stabiliser architecture*. Rsc Advances, 2014. **4**(87): p. 46876-46886.
19. Soares, J.L., et al., *Hydrotalcite materials for carbon dioxide adsorption at high temperatures: Characterization and diffusivity measurements*. Separation Science and Technology, 2004. **39**(9): p. 1989-2010.
20. Phongamwong, T., et al., *CO₂ hydrogenation to methanol over CuO-ZnO-ZrO₂-SiO₂ catalysts: Effects of SiO₂ contents*. Chemical Engineering Journal, 2017. **316**: p. 692-703.
21. Sun, P.H., et al., *A Highly Dispersed Copper Nanoparticles Catalyst with a Large Number of Weak Acid Centers for Efficiently Synthesizing the High Value-Added 3-Methylindole by Aniline and Biomass-Derived Glycerin*. Catalysis Letters, 2021. **151**(2): p. 463-477.
22. Li, S.Z., et al., *A highly active and selective mesostructured Cu/AlCeO catalyst for CO₂ hydrogenation to methanol*. Applied Catalysis a-General, 2019. **571**: p. 51-60.
23. Gao, P., et al., *Influence of Zr on the performance of Cu/Zn/Al/Zr catalysts via hydrotalcite-like precursors for CO₂ hydrogenation to methanol*. Journal of Catalysis, 2013. **298**: p. 51-60.

24. Ausavasukhi, A., et al., *Thermal transformation of copper incorporated hydrotalcite-derived oxides and their catalytic activity for ethanol dehydrogenation*. 2023. **117**: p. 371-385.
25. Tajrishi, O.Z., M. Taghizadeh, and A.D. Kiadehi, *Methanol steam reforming in a microchannel reactor by Zn-, Ce- and Zr-modified mesoporous Cu/SBA-15 nanocatalyst*. International Journal of Hydrogen Energy, 2018. **43**(31): p. 14103-14120.
26. Gonzalez-Arias, J., et al., *Valorization of biomass-derived CO₂ residues with Cu-MnOx catalysts for RWGS reaction*. Renewable Energy, 2022. **182**: p. 443-451.
27. Li, Z.P., et al., *Boosting CO₂ hydrogenation efficiency for methanol synthesis over Pd/In₂O₃/ZrO₂ catalysts by crystalline phase effect*. Applied Surface Science, 2022. **603**.
28. Jiang, F., et al., *Dependence of copper particle size and interface on methanol and CO formation in CO₂ hydrogenation over Cu@ZnO catalysts*. Catalysis Science & Technology, 2022. **12**(2): p. 551-564.
29. Zhang, X., et al., *Optimum Cu nanoparticle catalysts for CO₂ hydrogenation towards methanol*. Nano Energy, 2018. **43**: p. 200-209.
30. Burch, R., S.E. Golunski, and M.S. Spencer, *The Role of Copper and Zinc-Oxide in Methanol Synthesis Catalysts*. Journal of the Chemical Society-Faraday Transactions, 1990. **86**(15): p. 2683-2691.
31. Karelavic, A. and P. Ruiz, *The role of copper particle size in low pressure methanol synthesis via CO₂ hydrogenation over Cu/ZnO catalysts*. Catalysis Science & Technology, 2015. **5**(2): p. 869-881.

Improved copper-based catalysts for alcohol-assisted CO₂ hydrogenation: A comparative study between novel nano-stabilized and deposition-precipitation method

Supporting Information

Linlin Ye,^a Penny Xiao,^a Peter Scales,^c Ranjeet Singh,^a Paul Webley,^b Gang Kevin Li^{*a}

^a Department of Chemical Engineering, The University of Melbourne, Parkville, VIC 3010, Australia

^b Department of Chemical and Biological Engineering, Monash University, Wellington Rd, Clayton VIC 3800, Australia

^c ARC Centre of Excellence for Enabling Eco-Efficient Beneficiation of Minerals, Department of Chemical Engineering, The University of Melbourne, Parkville, VIC 3010, Australia

* Corresponding authors: li.g@unimelb.edu.au

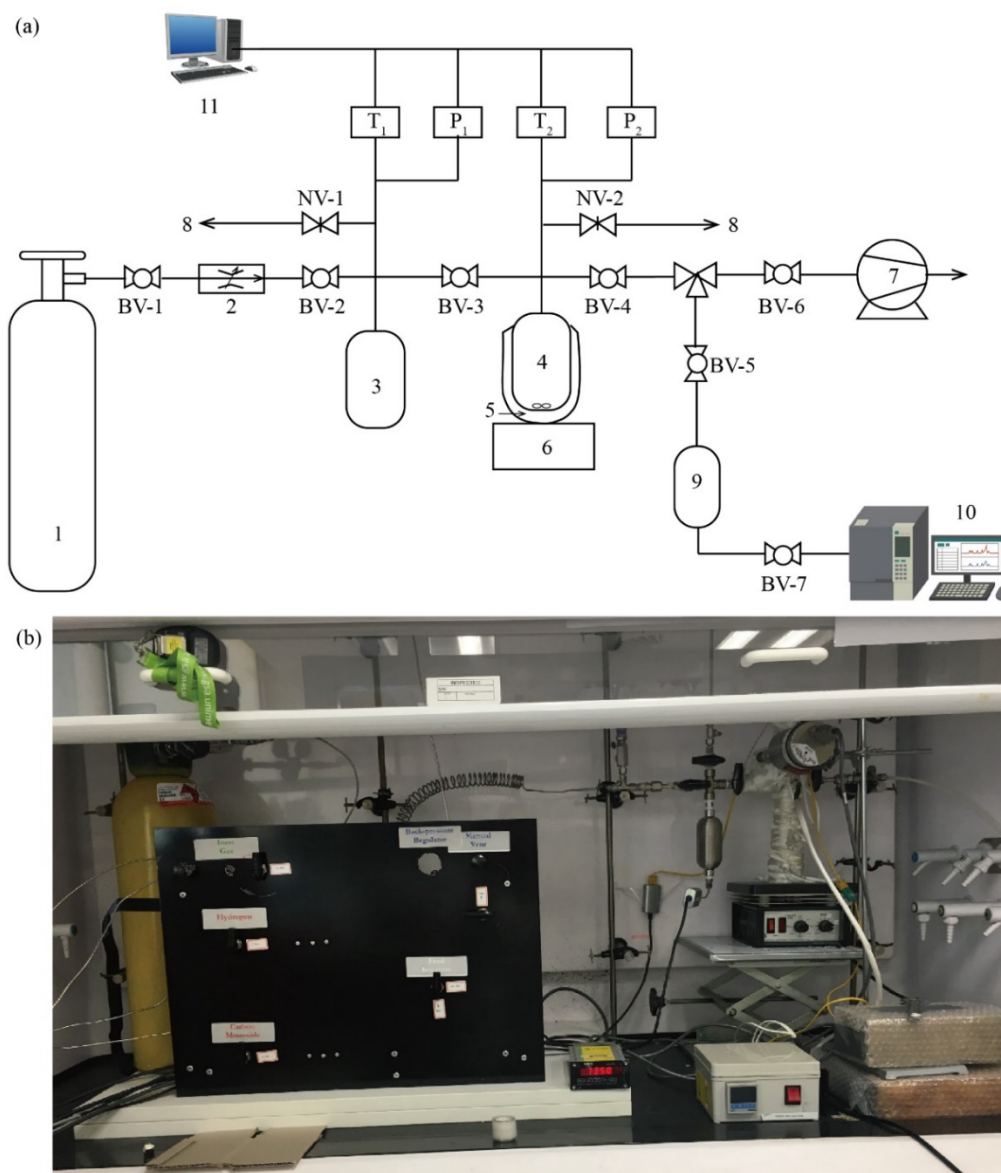


Figure S1. Reaction system. a) Schematic diagram of reaction apparatus 1. Gas cylinders (He, CO₂, H₂); 2. Mass flow controller, 3. Storage tank; 4. Reactor; 5. Heating tape/Cooling bath; 6. Magnetic stirrer; 7. Vacuum pump; 8. Vent system; 9. Gas sampling tank; 10. GC; BV-1 to BV-6: Ball valves; NV-1 to NV-2: Needle valves. b) Real reaction apparatus

EDS Analysis	Element	Weight Percentage (%)	Atom ratio (%)	Mg/Al (Atom ratio)	Zn/(Zn+Mg) (Atom ratio)
Before	Mg	54.29	57.19	1.34	N/A
	Al	45.71	42.81		
	Zn	N/A	N/A		
After	Mg	29.23	39.40	0.91	0.3
	Al	36.24	43.42		
	Zn	34.53	17.18		

Table S1. EDS analysis of supporting material HTC before and after ion-exchanged process

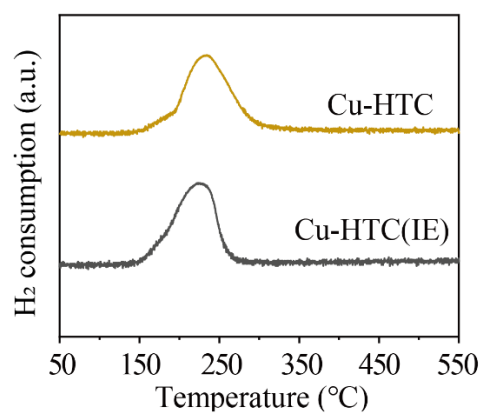


Figure S2. H₂-TPR profiles of the catalysts